Diamond Surface Modification to Enhance Interfacial Thermal Conductivity in Al/Diamond Composites

MARIO CACCIA,[1,2,3] ALEJANDRO RODRÍGUEZ,[1,2]
and JAVIER NARCISO[1,2]

1.—Instituto Universitario de Materiales de Alicante (IUMA), Alicante University, Alicante, Spain. 2.—Inorganic Chemistry Department, Alicante University, Alicante, Spain. 3.—e-mail: marioraul@ua.es

Diamond/metal composites are very attractive materials for electronics because their excellent thermal properties make them suitable for use as heat sink elements in multifunctional electronic packaging systems. To enlarge the potential applications of these composites, current efforts are mainly focused on investigating different ways to improve the contact between metal and diamond. In the present work, a theoretical study has been carried out to determine the differences between the interfacial thermal conductance of aluminum/diamond and aluminum/graphite interfaces. Additionally, diamond particles were surface modified with oxygen to observe how it affects the quality of the diamond surface. The characterization of the surface of diamonds has been performed using different surface analysis techniques, especially x-ray photoelectron spectroscopy and temperature-programmed desorption.

INTRODUCTION

The development of more powerful electronic devices has led to the need to obtain new materials with high thermal conductivity, tailored thermal expansion, reduced weight, and high stiffness. Novel materials constantly emerge to meet user demand, for instance, carbon matrix composites or metal matrix composites, overcoming the limitation of traditional materials. Owing to exceptionally high thermal conductivity, low thermal expansion, as well as low density, diamond seems to be a promising material to be used in electronic packaging. Furthermore, considering that the cost of good quality synthetic diamonds has been continuously decreasing during the past years, diamond has become an accessible material. One approach to transfer the attractive physical properties of diamond to bulk engineering components is to use diamond particles as a reinforcement material in a suitable metal matrix such as Al, Ag, or Cu.[1–3]

Diamond/metal composites are very attractive materials for electronic applications because their excellent thermal properties make them suitable for use as heat sink elements in multifunctional electronic packaging systems. To enlarge the potential applications of these composites, current efforts are mainly focused on investigating different ways to improve the thermal contact between metal and diamond. High thermal conductivity composites are usually prepared by infiltration.[4,5] This method consists of infiltrating a diamond preform with a liquid metal, e.g., Cu, Al, or Ag. Infiltration can be driven by mechanical forces (squeeze casting)[6,7] or by a pressure drop (gas pressure-assisted infiltration).[2] As these metals do not wet diamonds, the contact between reinforcement and matrix is deficient and needs to be improved to reach higher thermal conductivities. There are mainly three ways of achieving this.[8] One way of improving thermal contact between diamonds and metals is to add carbide-forming agents to form a barrier layer on the surface of diamonds. Aluminum, for example, is a carbide former, and the presence of Al_4C_3 has been observed in this kind of composite.[9,10] A drawback of this method is the slow rate of the process, and that temperatures at which reaction takes place for a wide spectrum of metallic alloys are high enough to degrade diamond to its allotropic graphite form, especially when diamonds contain oxygen on the surface. An alternative is to coat diamonds with carbide-forming agents to produce a

thin barrier layer on a diamond's surface prior to their infiltration with metal. A method was proposed[11] for titanium coating on particulate nanodiamonds from a NaCl + KCl + CaCl$_2$ blend at 750°C in argon atmosphere. Finally, a third method is to chemically modify the surface of diamond particles to improve diamond–metal interaction.

In this work, a theoretical study has been carried out to determine the differences between the interfacial thermal conductance (h_C) of aluminum/diamond and aluminum/graphite interfaces by using the acoustic-mismatch model (AMM).[12] In addition, experimental tests were performed in which diamond particles were surface modified with oxygen to observe how it affects the diamond surface. The characterization of the surface of diamonds has been performed using different surface analysis techniques, especially x-ray photoelectric spectroscopy (XPS) and temperature-programmed desorption (TPD). The thermal conductivity (K_c) of the final diamond/aluminum composites has been predicted using both Maxwell and Hasselman–Johnson predictive models.

THEORETICAL BACKGROUND

The thermal conductivity of metal matrix composites (MMCs) depends on many factors, such as phase properties and volume fractions, as well as on the geometric characteristics of the microstructure. In this material, the contact surface between metal and the reinforcement particles limits the thermal conductivity of the composites as it opposes a finite resistance (R_{BD}) to heat transfer from one phase to the other. The inverse of this resistance is known as interface thermal conductance (h_C). The interface thermal conductance, h_C, is generally defined as the ratio of the heat flux density (q) and the associated temperature drop (ΔT) across an interface as shown in Eq. 1:

$$h_C = \frac{1}{R_{BD}} = \frac{q}{\Delta T} \quad (1)$$

Among mean field predictions for thermal conductivity of composites (K_C), the scheme of Maxwell[13] is the most popular. This model corresponds to Eq. 2, where K_m is the thermal conductivity of the matrix; K_d^{eff} is the effective, size-dependent thermal conductivity of the particles; and V_d is the volume fraction of the particle:

$$K_C = \frac{K_m \times \left[2 \times K_m + K_d^{eff} + 2 \times \left(K_d^{eff} - K_m\right) \times V_d\right]}{2 \times K_m + K_d^{eff} - \left(K_d^{eff} - K_m\right) \times V_d} \quad (2)$$

For spherical particles, K_d^{eff} is also related to the intrinsic thermal conductivity (K_d^{in}) of the matter forming the particles[10] according to Eq. 3:

$$K_d^{eff} = \frac{K_d^{in}}{1 + \frac{K_d^{in}}{(r \times h_C)}} \quad (3)$$
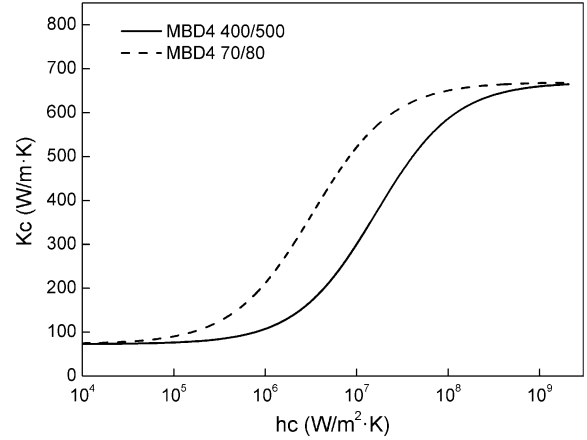

Fig. 1. Thermal conductivity of Al/diamond composites calculated with the Hasselman–Johnson model for two diamond particles of different sizes, as a function of interfacial thermal conductance.

where r is the radius of spherical particles and h_C is the interface thermal conductance. Combining Eqs. 3 and 2 results in the Hasselman–Johnson model for composites with finite interfacial thermal resistance.[14] Figure 1 shows the dependence of K_c with h_C, calculated using this model for two composites made of aluminum and two different sizes of MBD4 diamonds (47 μm and 228 μm). The smaller ones are characterized further on.

It is observed that for low h_C values, the model does not depend on the particle diameter. However, for values of h_C between 1×10^5 W/m·K and 1×10^8 W/m·K, the model shows significant differences depending on the particle's diameter. When the value of h_C becomes larger, the model becomes again independent of the particle size. Typical values for h_C for Al/diamond composites are between 1×10^7 W/m·K and 1×10^8 W/m·K so the model is sensitive to the particle size for this kind of composite.

To calculate h_C, the AMM has been applied. This first-order method is considered a good approximation at low temperature and smooth interfaces.[15,16] For this model, h_C is given by Eq. 4, where C_p is the specific heat per volume of the metal matrix, η_{1-2} is the transmission coefficient of phonons across the interface from 1 to 2 (metal to particle), and C_D is the Debye velocity of the metal:

$$h_C = \frac{1}{4} \times C_p \times \eta_{1-2} \times C_D \quad (4)$$

C_D is given by Eq. 5, where c_l and c_t are, respectively, the longitudinal and transversal phonon velocities across the metal.

$$c_D = \frac{1}{\sqrt{\frac{1}{2} \times \left(\frac{1}{c_l^2} + \frac{1}{c_t^2}\right)}} \quad (5)$$

The AMM treats the interface transfer problem in terms of continuum mechanics.[16] An incoming

Table I. Density, phonon velocity, Debye velocity, and specific heat for the different materials[12–14]

Material	ρ (kg/m^3)	c_l (m/s)	c_t (m/s)	C_D (m/s)	C_p (J/m^3·K)
Aluminum	2700	6240	3400	3865	2.44×10^6
Diamond	3512	20000	12300	14817	–
Graphite	2300	17500	12800	14611	–

elastic phonon wave at an interface can only be transmitted if it arrives at a critical angle; otherwise, the wave is completely reflected. In addition, elastic waves arriving with the critical angle can be either reflected or transmitted, depending on the acoustic impedance of the two materials forming the interface. The transmission coefficient for the AMM is given by Eq. 6, where p is the transmission probability of incident phonons with the critical angle; q is the fraction of such phonons among all incident ones; Z_i is the acoustic impedance ($Z = \rho \times c$) for each phase with i = 1, 2; and c_i is the sound velocity for each phase with i = 1, 2.

$$\eta_{1-2} = p \times q = \frac{2 \times Z_1 \times Z_2}{(Z_1 + Z_2)^2} \times \left(\frac{c_1}{c_2}\right)^2 \quad (6)$$

Table I presents the parameters used to estimate the h_C between aluminum (Al) and diamond (D) particles and between aluminum (Al) and graphite (Gr).

Table II shows the calculations of h_C for the different composites. It can be observed that thermal interfacial conductance for Al/Gr doubles the value for Al/D, which can be translated in a better thermal joint between the metal matrix and the reinforcement particles. According to these calculations, the surface modification of diamond particles to obtain an sp^2 structure would result in an improvement in the thermal contact with the metal and, hence, in improvement in the thermal conductivity of the final composite. It must be pointed out that the phonon velocity value for graphite used to calculate the η_{1-2} for Al/Gr is not the Debye velocity but the transversal velocity. When modifying the surface of diamond, it is reasonable to assume that graphite sheets will grow parallel to the diamond surface, so it would be more accurate to use the transversal phonon velocity rather than the Debye velocity.

EXPERIMENTAL PROCEDURES

Diamonds

In this work, synthetic diamonds of type Ib (MDB4 grade 400/500 mesh) were used. These diamonds were produced using the high pressure high temperature process and present a cubo-octahedral geometry.

Particle Size Distribution

Particle size distribution was obtained using a Coulter laser particle analyzer. Volume statistics

Table II. Calculations of h_C for the different interfaces

Composite	η_{1-2}	h_C (W/m^2·K)
Al/Gr	0.039	9.29×10^7
Al/D	0.020	4.63×10^7

were obtained using the software provided with the equipment.

Density of the Particles

The density of the particles was determined using helium picnometry. These tests were carried out in a Micrometrics Accupyc 1330TC device.

Scanning Electron Microscopy

Scanning electron microscopy (SEM) images were obtained using a Hitachi electronic microscope model S3000N with a Brucker x-ray detector model XFlash 3001 for microanalysis (EDS) and Mapping.

X-ray Photoelectric Spectroscopy

The x-ray photoelectric spectroscopy (XPS) spectra have been obtained with a VG-Microtech Multilab electron spectrometer by using the Mg Kα (1253.6 eV) radiation of a twin anode in the constant analyzer energy mode with a pass energy of 50 eV. The pressure of the analysis chamber was maintained at 10^{-5} mbar. The binding energy and the Auger kinetic energy scale were calibrated by setting the C1s transition at 284.6 eV. The accuracy of BE and KE values was ±0.2 eV and ±0.3 eV, respectively. The BE and KE values were obtained by using the Peak-fit Program implemented in the control software of the spectrometer

Temperature-Programmed Desorption

Temperature-programmed desorption (TPD) tests were performed in a U-shaped quartz cell. Samples were treated at 373 K for 1 h under a helium flow, with a flow rate of 50 cm^3/min. Then, the temperature was raised at a rate of 10°C/min up to 1025°C. The decomposition products (carbon monoxide, carbon dioxide, and water) were monitored by on-line mass spectrometry, with a Pfeiffer mass spectrometer model Omnistar^{TM}.

Table III. Characteristics of diamond particles and particle size distribution

Diamond	$D(90)$ (μm)	$D(50)$ (μm)	$D(10)$ (μm)	$D(4,3)$ (μm)	$D(3,2)$ (μm)	Span	ρ (g/cm^3)	V_d
MBD4 400/500	61.59	46.22	35.03	47.23	45.27	0.57	3.51	0.61

V_d is the particle volume fraction used for thermal conductivity calculations, the parameter $D(50)$ represents the median of the particle size distribution, $D(90)$ and $D(10)$ are the 10 and 90 percentiles, the span is a measure of the particle distribution width calculated as $D(90) - D(10)/D(50)$, ρ is the skeletal density of the particles, and $D(4,3)$ and $D(3,2)$ are the volume and surface mean values.
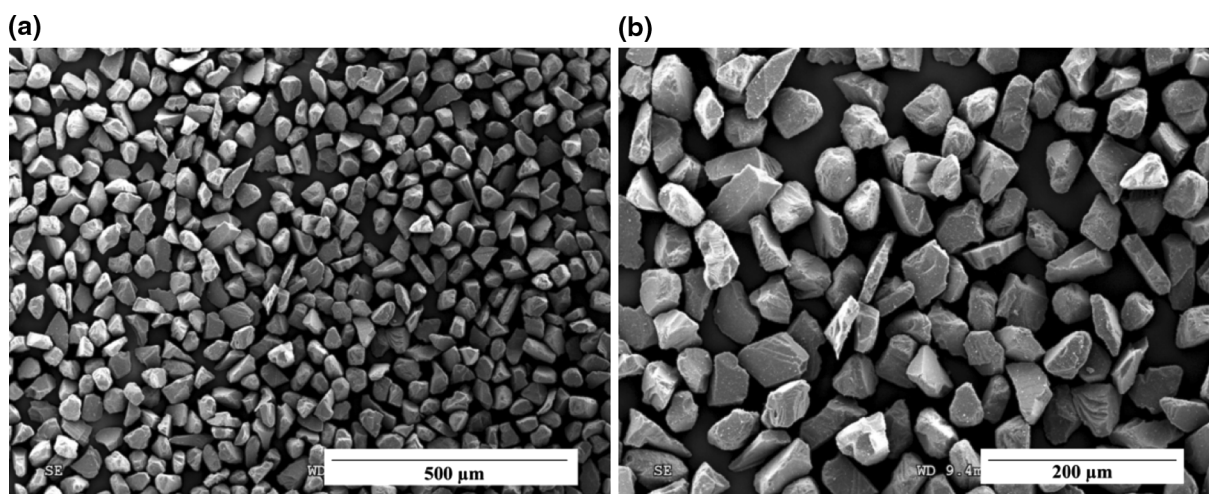
(a) **(b)**

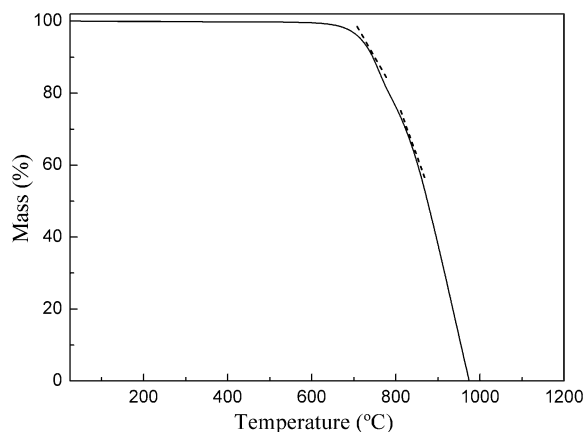Fig. 2. SEM images of the MBD4 400/500 diamond particles used for surface modifications.

Fig. 3. TGA of MBD4 400/500 diamonds in air. Two different slopes are observed corresponding to the different reactivity of {111} and {001} faces.

Thermogravimetric Analysis

The thermogravimetric analysis (TGA) tests were performed in a Mettler Toledo TG–DTA model TGA/SDTA851e/LF/1600 device. Tests were performed in air atmosphere with a temperature range from 25°C to 1200°C, and a heating rate of 10°C/min.

Surface Modification

MBD4 400/500 diamond particles were heat treated at 500°C in an oxygen atmosphere, with a flow rate of 60 cm^3/min, maintaining maximum temperature for 90 min, in a horizontal tube furnace Carbolite model STF 16/75/450.

RESULTS AND DISCUSSION

Diamond Characterization

The main characteristics of diamonds are shown in Table III. Particles present a narrow size distribution, which is depicted by the low value of the span. In addition to the fact that $D(4,3)$ and $D(3,2)$ are relatively similar to $D(50)$, the particle size distribution is quite symmetric.

The geometry of the diamond particles can be observed in SEM images in Fig. 2. It is observed that MBD4 400/500 exhibit various geometries from almost round particles to very elongated ones.

X-ray diffraction (XRD) and Raman spectroscopy show that diamond is the only crystalline phase present in the reinforcement particles. TGA in air shows two different slopes, which correspond to the different crystallographic faces of diamond, {111} and {001}, which have different reactivity, with {100} being the most reactive. So the first mass loss corresponds to the oxidation of the {100} face, and the second mass loss corresponds to the oxidation of {111} face. In Fig. 3, the TGA of diamonds MBD4 400/500 is shown as an example.
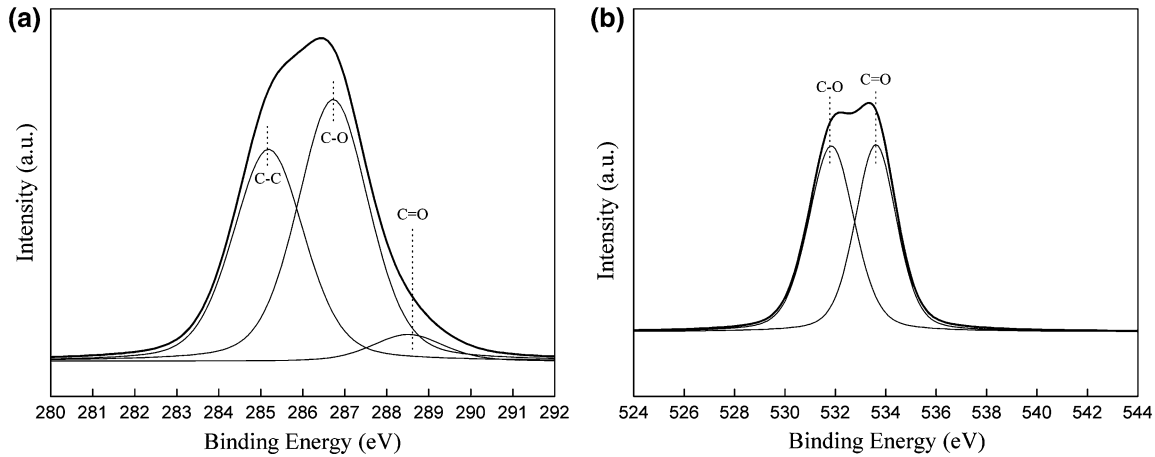
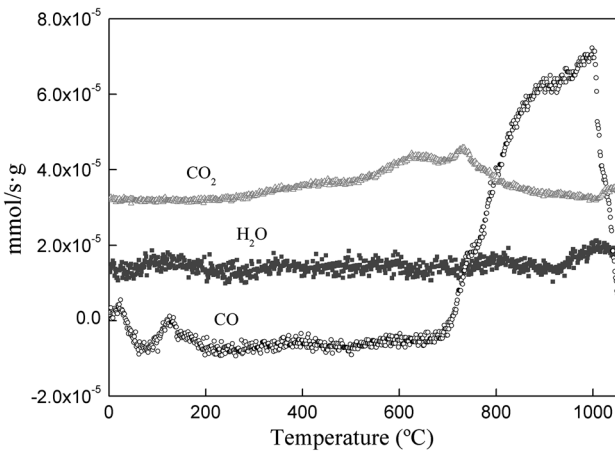Fig. 4. Deconvolution of C1s (a) and O1s (b) XPS spectra of MBD4 400/500 as-received diamonds.

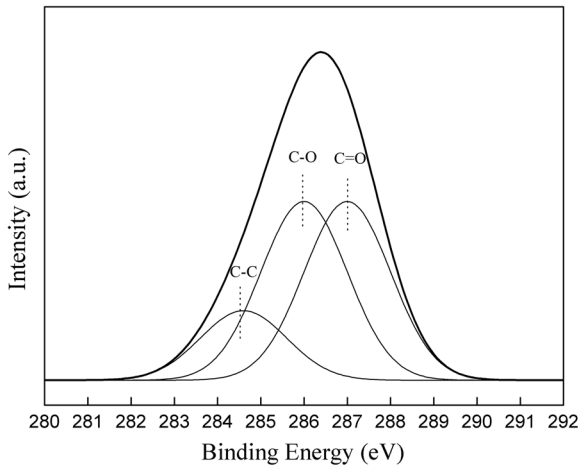Fig. 5. TPD curves for MBD4 400/500 diamonds.

Fig. 6. Deconvolution of C1s XPS spectra of MBD4 400/500 surface-modified diamonds.

Surface Characterization

The XPS spectrum of C1s, shown in Fig. 4, indicates that the diamond surface presents an sp^3 structure, represented by the peak at 285 eV with oxygen adsorbed represented by the peaks at 286.6 eV and 288.5 eV. O1s spectra show two peaks at 532 eV and 534 eV usually associated with a single and double carbon–oxygen bond, e.g., lactone and carbonyl groups. Clean sp^3 carbon represents 42% of the surface of diamonds.

Oxygen chemisorbed on the surface of diamond has formed a chemical bond with surface atoms and will therefore not desorb as molecular oxygen but as CO or CO_2.[17] Figure 5 shows the TPD profiles for H_2O, CO and CO_2. No H_2O desorption is observed. CO_2 desorption is observed at low temperatures (500°C) as expected from lactone groups, while CO desorption is observed at higher temperatures (800–1000°C), as expected from carbonyl groups.[18]

Surface Modification

Figure 6 shows the C1s XPS spectra of surface-modified MBD4 diamonds after being heat treated with oxygen at 500°C for 90 min. The temperature of the treatment was selected to ensure maximum oxygen chemisorption without carbon combustion. It is observed that the 285-eV peak has shifted to lower binding energies associated with an sp^2 structure at around 284.6 eV. Two other peaks are observed at higher binding energies, which are associated with adsorbed oxygen. This means that diamond surface oxidation has transformed the surface of diamond particles from an sp^3 structure to an sp^2 one. As demonstrated before, the Al/graphite interface has a higher interfacial thermal conductance and hence is more appropriate for Al/diamond composites.

Table IV shows the calculations of K_C for aluminum/diamond composites made of MBD4 400/500 diamond particles, both as received and surface modified, and pure aluminum, using the Maxwell and the Hasselman-Johnson models. The value of K_d^{in} for MBD4 diamonds, used for these calculations, has been measured by Molina et al.[1] It is depicted

Table IV. Thermal conductivity predictions for Al/diamond composites with as-received and surface-modified diamonds for different models

Model	Interface	K_C (W/m·K)
Maxwell	Al/diamond	669
	Al/graphite	669
Hasselman–Johnson	Al/diamond	515
	Al/graphite	590

V_d used for calculations is 0.6.

that the Maxwell model, which does not take into account the interfacial effect, provides an overestimation of the thermal conductivity of the composite, and shows no difference for as-received and surface-modified diamonds. The Hasselman–Johnson model shows a more realistic thermal conductivity for the composite, and the thermal conductivity improvement when using surface-modified diamonds becomes evident.

CONCLUSION

A method was proposed to modify the surface of diamond particles to obtain an sp^2 structure thermally more compatible with an aluminum matrix. Theoretical calculations show that the sp^2/Al interface presents a higher interfacial thermal conductance than the diamond sp^3/Al interface, and predictive models suggest that better thermal conductivity in Al/diamond composites will be obtained with this surface modification.

REFERENCES

1. J.M. Molina, M. Rhême, J. Carron, and L. Weber, *Scr. Mater.* 58, 393 (2008).
2. C. García-Cordovilla, E. Louis, and J. Narciso, *Acta Mater.* 47, 4461 (1999).
3. R. Prasher, *Phys. Rev. B* 77, 1 (2008).
4. S.V. Kidalov and F.M. Shakhov, *Materials* 2, 2467 (2009).
5. J.M. Molina, R.A. Saravanan, R. Arpón, C. García-Cordovilla, E. Louis, and J. Narciso, *Acta Mater.* 50, 247 (2002).
6. A. Rodríguez-Guerrero, S.A. Sánchez, J. Narciso, E. Louis, and F. Rodríguez-Reinoso, *Acta Mater.* 54, 1821 (2006).
7. A. Rodríguez, S.A. Sánchez, J. Narciso, E. Louis, and F. Rodríguez-Reinoso, *J. Mater. Sci.* 40, 2519 (2005).
8. C. Monachon and L. Weber, *Diamond Relat. Mater.* 39, 8 (2013).
9. I.E. Monje, E. Louis, and J.M. Molina, *Compos. A* 48, 9 (2013).
10. S. Kleiner, F.A. Khalid, P.W. Ruch, S. Meierb, and O. Befforta, *Scr. Mater.* 55, 291 (2006).
11. E. Breval, J. Chang, and D.K. Agrawal, *J. Am. Ceram. Soc.* 83, 2106 (2000).
12. M. Kida, L. Weber, C. Monachon, and A. Mortensen, *J. Appl. Phys.* 109, 1 (2011).
13. J.C. Maxwell, *Treatise on Electricity and Magnetism*, 3rd ed. (New York: Dover, 1954).
14. D.P.H. Hasselman and L.F. Johnson, *J. Compos. Mater.* 21, 508 (1987).
15. E.T. Swartz (Ph.D. dissertation, Cornell University, 1987).
16. E.T. Swartz and R.O. Pohl, *Rev. Mod. Phys.* 61, 605 (1989).
17. F. Rodríguez-Reinoso and M. Molina-Sabio, *Adv. Colloid Interface Sci.* 76–77, 271 (1998).
18. F. Rodríguez-Reinoso, M. Molina-Sabio, and M.T. González, *Langmuir* 13, 2354 (1997).